Intramembrane binding of VE-cadherin to VEGFR2 and VEGFR3 assembles the endothelial mechanosensory complex

Brian G. Coon,[1,2] Nicolas Baeyens,[1,2] Jinah Han,[1,2] Madhusudhan Budatha,[1,2] Tyler D. Ross,[1,2] Jennifer S. Fang,[1,2] Sanguk Yun,[1,2] Jeon-Leon Thomas,[3,4,5,8] and Martin A. Schwartz[1,2,6,7]

[1]Yale Cardiovascular Research Center and [2]Department of Internal Medicine, Cardiovascular Medicine, Yale University School of Medicine, New Haven, CT 06510
[3]Université Pierre and Marie Curie–Paris 6, 75005 Paris, France
[4]Institut National de la Santé et de la Recherche Médicale/Centre National de la Recherche Scientifique U-1127/UMR-7225, 75654 Paris, France
[5]Assistance Publique–Hôpitaux de Paris, Groupe Hospitalier Pitié-Salpètrière, 75013 Paris, France
[6]Department of Cell Biology, [7]Department of Biomedical Engineering, and [8]Department of Neurology, Yale University, New Haven, CT 06520

Endothelial responses to fluid shear stress are essential for vascular development and physiology, and determine the formation of atherosclerotic plaques at regions of disturbed flow. Previous work identified VE-cadherin as an essential component, along with PECAM-1 and VEGFR2, of a complex that mediates flow signaling. However, VE-cadherin's precise role is poorly understood. We now show that the transmembrane domain of VE-cadherin mediates an essential adapter function by binding directly to the transmembrane domain of VEGFR2, as well as VEGFR3, which we now identify as another component of the junctional mechanosensory complex. VEGFR2 and VEGFR3 signal redundantly downstream of VE-cadherin. Furthermore, VEGFR3 expression is observed in the aortic endothelium, where it contributes to flow responses in vivo. In summary, this study identifies a novel adapter function for VE-cadherin mediated by transmembrane domain association with VEGFRs.

Introduction

Endothelial cells (ECs) are highly responsive to fluid shear stress from blood flow, activating a large number of signaling and gene expression pathways depending on the magnitude, pulsatility, and direction of the flow (Davies, 1995; Chiu et al., 2009; Chiu and Chien, 2011). These signals are crucial for embryonic development, including the rearrangement of the primitive vascular plexus into a vascular tree (Lucitti et al., 2007), development of the heart (Hove et al., 2003), and several aspects of adult physiology. Increases or decreases in fluid shear stress magnitude induce, respectively, vasorelaxation or constriction on short time scales, and outward or inward vessel remodeling on longer time scales (Langille and O'Donnell, 1986; Pohl et al., 1986; Di Stefano et al., 1998). Furthermore, high laminar or pulsatile fluid flow inhibits proliferation and activation of inflammatory pathways in the endothelium to stabilize the vasculature (Mattsson et al., 1997; Tedgui and Mallat, 2001; Nayak et al., 2011; Gimbrone and García-Cardeña, 2013). In contrast, low, oscillatory, or multidirectional fluid shear stress (termed disturbed flow) activates inflammatory pathways including NF-κB and JNK (Dai et al., 2004; Orr et al., 2008; Hahn et al., 2009; Hahn and Schwartz, 2009; Nigro et al., 2011). These pathways stimulate expression of cytokines and adhesion receptors such as MCP-1, VCAM-1, and ICAM-1 that mediate recruitment of leukocytes. This differential activation of pro- versus anti-inflammatory pathways is believed to underlie the preferential occurrence of atherosclerotic plaque at regions of artery branching, bifurcation, and high curvature that have lower flow and complex, multidirectional flow patterns.

Previous work identified a complex of proteins at cell–cell junctions, consisting of PECAM-1, VE-cadherin (VEcad), and VEGFR2, as an important, endothelial-specific flow sensor (Tzima et al., 2005). PECAM-1 is an Ig family homophilic cell adhesion receptor that localizes to endothelial cell–cell contacts and contributes to junctional integrity and movement of

Correspondence to Martin A. Schwartz: Martin.Schwartz@yale.edu

Abbreviations used in this paper: EGCS, endothelial cell growth supplement; HUVEC, human umbilical cord endothelial cell; Ncad, N-cadherin; OSS, oscillatory shear stress; SFK, Src family kinase; TMD, transmembrane domain; VEcad, VE-cadherin; VEGFR, vascular endothelial growth factor receptor; WT, wild type.

The Rockefeller University Press $30.00
J. Cell Biol. Vol. 208 No. 7 975–986
www.jcb.org/cgi/doi/10.1083/jcb.201408103

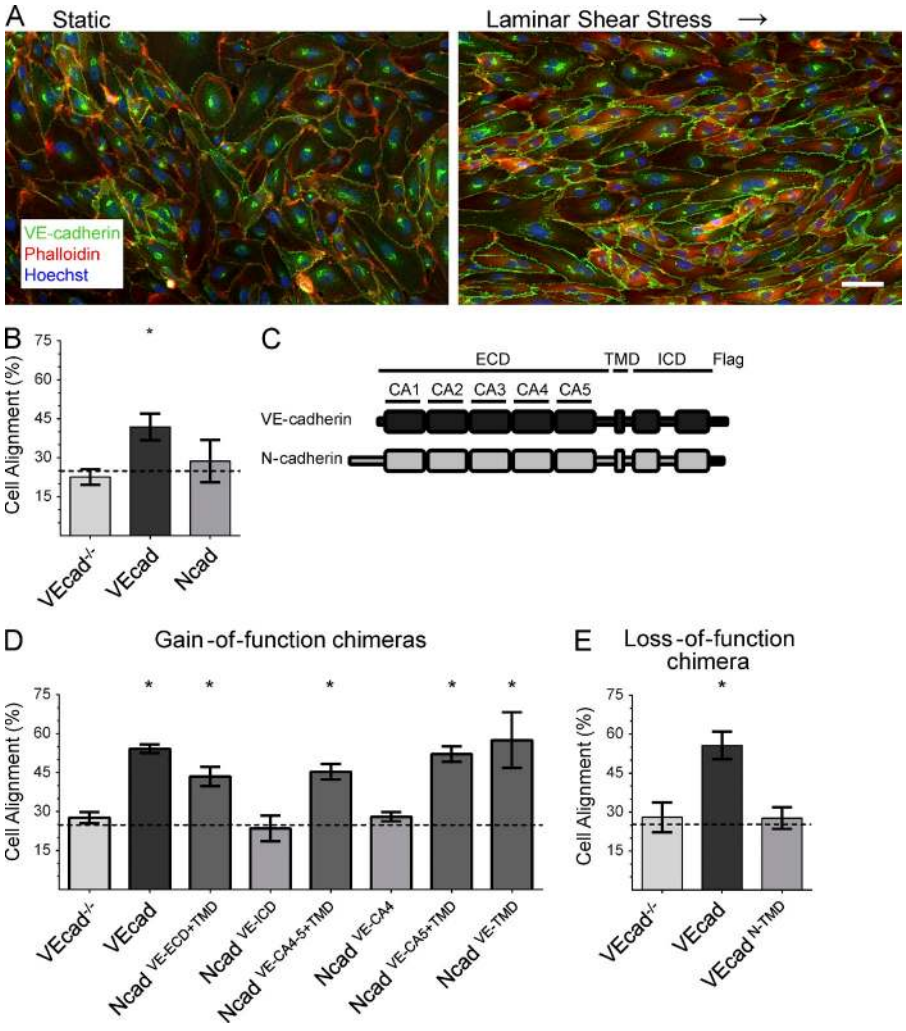

Figure 1. **Using cadherin chimeras to map VEcad-specific functional domains.** (A) Endothelial cells orient into the direction of flow. Shown is an example of shear-induced alignment in HUVECs after exposure to 12 dynes/cm^2 laminar shear stress for 16 h in a parallel plate flow chamber. Slides were fixed and stained for VEcad, phalloidin–Alexa Fluor 647, and Hoechst. Bar, 30 µm. (B) VEcad-null (VEcad$^{-/-}$) endothelial cells were reconstituted with human VEcad or Ncad, then exposed to 12 dynes/cm^2 laminar shear stress for 16 h. Cell alignment in the direction of flow (±23°) was quantified. Values are means ± SEM (error bars), $n \geq 3$. (C) Domain organization of VEcad and Ncad. Each cadherin has an extracellular domain containing five cadherin repeats (CA1–5), a single-pass TMD, and an intracellular domain (ICD) including p120 and β-catenin binding sites. A Flag tag was also added to each construct. (D) VEcad$^{-/-}$ cells reconstituted with WT or chimeric VEcad/Ncad were assayed for alignment as in B. (E) VEcad$^{-/-}$ cells were reconstituted with mouse, WT VEcad, or VEcad containing the human Ncad-TMD (VEcad$^{N\text{-}TMD}$). Alignment in flow was analyzed as in A. Values are means ± SEM (error bars), $n \geq 3$. *, $P < 0.05$ significance to VEcad$^{-/-}$ by one-way analysis of variance (ANOVA). The broken lines in each graph indicate random alignment.

leukocytes across the endothelium (Privratsky et al., 2010). It is dispensable for embryonic development but is required for flow-induced vessel remodeling and contributes to inflammatory activation at regions of disturbed flow and atherosclerosis (Goel et al., 2008; Harry et al., 2008; Stevens et al., 2008). Development of a molecular force sensor showed that application of flow to ECs induces piconewton force across PECAM-1 (Conway et al., 2013), while direct application of force to PECAM-1 triggers some of the same pathways that are activated by flow (Osawa et al., 2002; Tzima et al., 2005). Thus, PECAM-1 appears to be a true mechanotransducer for fluid shear stress. VEcad is a classical type II cadherin that localizes to endothelial cell junctions and is essential for vascular development and integrity (Vestweber, 2008). Its deletion is embryonic lethal in part due to a defect in vascular endothelial growth factor receptor (VEGFR) signaling, which indicates an interaction between these receptors (Carmeliet et al., 1999). It is also essential for ligand-independent activation of VEGFR2 by flow, though the nature of this requirement is poorly understood (Tzima et al., 2005). VEcad does not show any increase in tension after flow (Conway et al., 2013), does not activate relevant pathways when tension is applied through magnetic beads (Tzima et al., 2005), and thus does not directly transduce mechanical forces. Yet, it is essential for downstream signaling when tension is applied to PECAM-1 (Tzima et al., 2005). VEcad is not strictly required for endothelial cell junction formation per se, since its loss results in up-regulation of N-cadherin (Ncad; Navarro et al., 1998; Giampietro et al., 2012), which indicates that flow signaling is a VEcad-specific function.

Our current model for flow signaling through the junctional complex is that force on PECAM-1 triggers activation of a Src family kinase (SFK), probably Fyn (Chiu et al., 2008), which phosphorylates and activates VEGFR2 in the absence of ligand. Activated VEGFR2 triggers multiple downstream pathways including PI 3-kinase (Jin et al., 2003), which stimulates conversion of integrins to the high-affinity conformation, binding to extracellular matrix and downstream signaling (Orr et al., 2006). Integrin signaling mediates alignment of the ECs in the direction of flow, and, depending on the extracellular matrix, the activation or suppression of inflammatory pathways (Orr et al., 2005, 2006, 2008; Hahn et al., 2009, 2011). Stimulation of PI 3-kinase though this pathway is also important for activation of eNOS and vasorelaxation (Fleming et al., 2005). In laminar flow, inflammatory activation is transient, followed by alignment of the cells in the direction of flow, down-regulation of inflammatory pathways, and up-regulation of anti-inflammatory

pathways (Hwang et al., 2003; Hahn et al., 2011; Wang et al., 2013). In contrast, in disturbed flow, cells do not align and inflammatory activation is sustained (Hwang et al., 2003; Cicha et al., 2008; Feaver et al., 2010; Wang et al., 2013).

In this study, we set out to understand VEcad's precise role in shear stress signaling. We took advantage of the fact that its close paralogue Ncad can mediate endothelial cell–cell junctions but not flow signaling. VEcad/Ncad chimeras identified the transmembrane domain (TMD) as the critical VE-specific region required for flow signaling. Subsequent work showed that this region binds VEGFR2 and -3, and demonstrated a role for VEGFR3 in flow signaling in vitro and in vivo.

Results

The VEcad TMD is required for shear mechanotransduction

To confirm that VEcad is unique in its involvement in shear stress signaling and to validate the experimental system, VEcad-null endothelial cells ($VEcad^{-/-}$; Carmeliet et al., 1999) were infected with lentivirus coding for with either VEcad or Ncad. Cells showing equal expression were selected (Fig. S1 A) and used for subsequent studies. Both cadherins localized well to cell–cell borders and bound β-catenin similarly (Fig. S1 B). To assess flow responsiveness, we examined alignment after 18 h of flow at 12 dynes/cm^2 (Fig. 1 A). Only VEcad rescued the alignment defect of $VEcad^{-/-}$ cells (Fig. 1 B). Next, we used this assay to examine chimeras with different regions of VEcad and Ncad (see Fig. 1 C for domain organization). All of the chimeric cadherins also localized well to cell–cell contacts and bound β-catenin (Fig. S1, B and C; and data not depicted). The first round of experiments showed that a segment comprising the extracellular domain (ECD) and TMD of VEcad conferred flow sensitivity, whereas the cytoplasmic domain did not (Fig. 1 D). Further dissection of the extracellular/transmembrane regions showed that the transmembrane sequence of VEcad fully rescued alignment when inserted into Ncad ($Ncad^{VE\text{-}TMD}$; Fig. 1 D). Conversely, substitution of the Ncad TMD into VEcad ($VEcad^{N\text{-}TMD}$) completely abrogated alignment (Fig. 1 E).

We next examined additional flow responses through the junctional complex. VEcad was previously reported to be downstream of shear-induced SFK activation but upstream of VEGFR2 activation (Tzima et al., 2005). We first confirmed this using VEcad knockdown in human umbilical cord endothelial cells (HUVECs). Cells expressing control or anti-VEcad shRNA were treated with laminar shear stress for 1 min. Shear stress activated SFK in both cells but VEGFR2 was only activated in control cells (Fig. 2 A). We then tested VEGFR2 transactivation in our chimeric cadherin-expressing cells. Onset of laminar flow transactivated VEGFR2 in cells expressing wild-type (WT) VEcad or $Ncad^{VE\text{-}TMD}$, but not Ncad or $VEcad^{N\text{-}TMD}$ (Fig. 2 B). Phosphorylation of the PI 3-kinase p85 subunit by onset of flow showed similar characteristics (Fig. 2 C). Together, these data show that the VEcad TMD is the critical VE-specific region required for responses to fluid shear stress through the junctional complex.

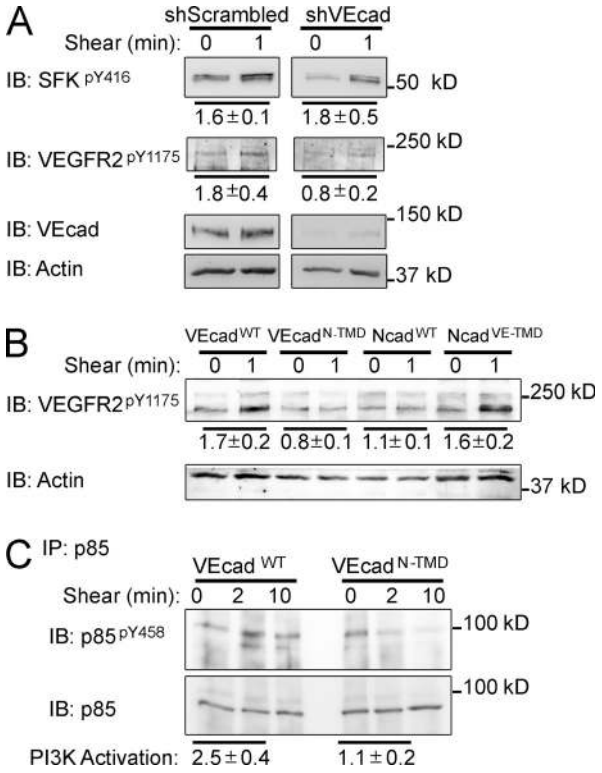

Figure 2. **VEcad TMD in flow signaling.** (A) Requirement for VEcad. HUVECS were infected with scrambled or anti-VEcad shRNA-containing lentiviruses then subjected to 12 dynes/cm^2 laminar shear for 1 min. Activation of SFKs (SFK^{pY416}, ~55 kD) and VEGFR2 ($VEGFR2^{pY1175}$, ~250 and 220 kD) were assayed by immunoblotting, with actin as a loading control. (B) VEcad TMD requirement for VEGFR activation. $VEcad^{-/-}$ cells reconstituted with $VEcad^{WT}$, $Ncad^{VE\text{-}TMD}$, $Ncad^{WT}$, and $VEcad^{N\text{-}TMD}$ were subjected to laminar shear stress for 1 min, then VEGFR2 activation was assayed as in A. (C) VEcad requirement for PI3K signaling. Cells were subjected to laminar shear stress, then p85 immunoprecipitated and immunoblotted with anti-$p85^{pY458}$ antibody. Values beneath each panel indicate phosphorylation relative to cells without flow, quantified by densitometry with total p85 serving as a loading control. For all panels, values are means ± SEM, $n = 3$. IB, immunoblotting.

The VEcad TMD confers binding to VEGFR2 and VEGFR3

We next addressed how the VEcad TMD might contribute to flow signaling. We previously hypothesized that VEcad functioned as an adapter in this pathway (Tzima et al., 2005). Therefore, we tested for protein interactions specific to this sequence. Immunoprecipitates from both $Ncad^{VE\text{-}TMD}$ chimera and Ncad were examined by SDS-PAGE and silver staining. A weak band at 190 kD in the $Ncad^{VE\text{-}TMD}$ chimera and absent in the Ncad immunoprecipitates was cut from the gel and subjected to mass spectrometry protein identification. The band contained multiple peptides from VEGFR3, a close homologue of VEGFR2 (Fig. S2 A). To confirm this result, we immunoprecipitated either endogenous VEcad or Ncad from HUVEC lysates. An equivalent amount of β-catenin was detected in both immunoprecipitates, which indicates that the same amount of each cadherin was isolated (Navarro et al., 1998). However, VEGFR3 immunoprecipitated with VEcad but not Ncad (Fig. 3 A). This interaction was constitutive, as no increase was observed in response to flow (Fig. S2 B). To further test the specificity of the interaction,

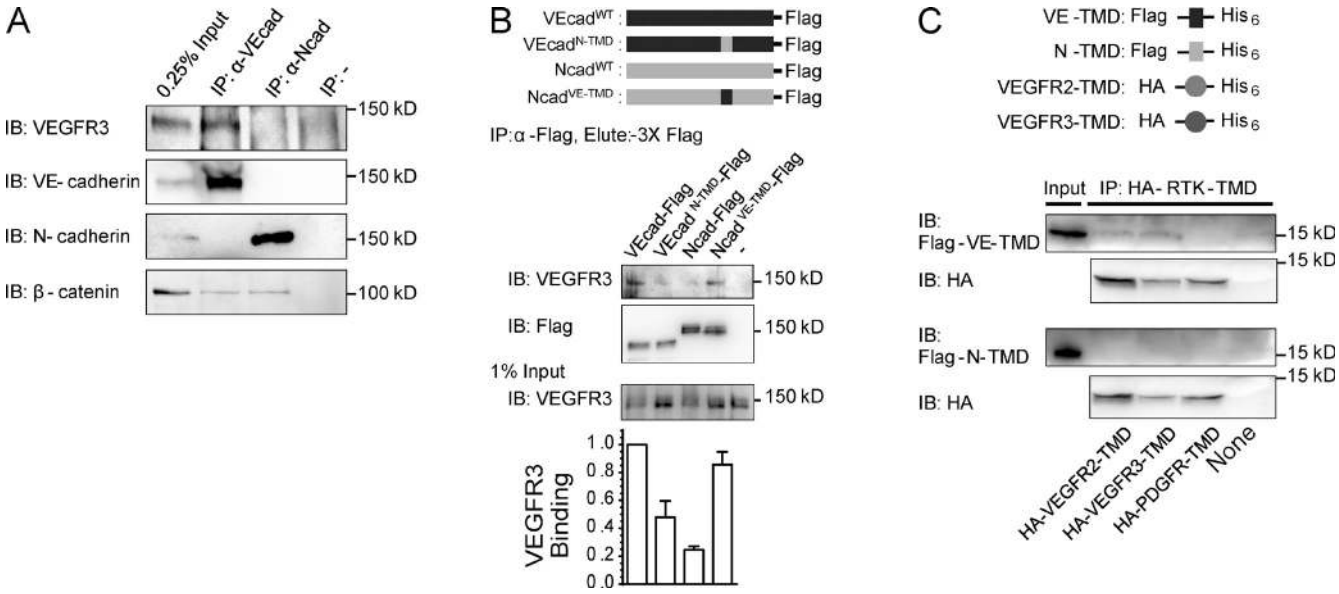

Figure 3. **Interaction of VEGFRs with VEcad through the TMDs.** (A) Coimmunoprecipitation of endogenous VEcad with VEGFR3. Lysates from confluent HUVECs were immunoprecipitated for VEcad, Ncad, or with control antibody and immunoblotted for VEGFR3. β-Catenin was used as a loading control. (B) Dependence on the TMD. VEGFR3-GFP was cotransfected with Flag-tagged cadherins into Cos7 cells, then cells were lysed, immunoprecipitated for Flag, and eluted with 3×-Flag peptide. Eluted proteins were analyzed by immunoblotting as indicated. Relative binding was measured by densitometry, and quantification is shown in the graph below. Values are means ± SEM (error bars), $n = 4$. (C) Direct binding. HA-tagged VEGFR or PDGFRβ and Flag-tagged cadherin TMD constructs are depicted in the top panel. Proteins were purified, mixed, and immunoprecipitated with anti-HA–coupled Protein A/G agarose. Immunoprecipitates were analyzed by immunoblotting for Flag and HA. Results in A–C are representative of at least three independent experiments. IB, immunoblotting.

immunoprecipitates for Flag-tagged VEcad and Ncad, and the Ncad$^{VE\text{-}TMD}$ and VEcad$^{N\text{-}TMD}$ chimeras, were probed for VEGFR3. Both VEcad and Ncad$^{VE\text{-}TMD}$ bound VEGFR3 at significantly greater levels than Ncad and VEcad$^{N\text{-}TMD}$, which indicates that the interaction is primarily driven by the VE-TMD (Fig. 3 B). The VE-TMD–containing constructs also coimmunoprecipitated with VEGFR2 (Fig. S2 C), although, in HUVEC lysates, this interaction appeared weaker than for VEGFR3. Thus, the VEcad TMD mediates the interaction with VEGFRs.

We also attempted to validate this interaction by colocalization to endothelial cell–cell junctions. However, the results were hard to interpret, probably due to cell geometry that causes many membrane proteins to appear brighter at cell–cell contacts. We therefore examined colocalization of VEGFR3-GFP and VEcad by plating VEcad^{WT} and VEcad$^{N\text{-}TMD}$ cells on slides coated with immobilized VEcad extracellular domain-Fc. Cells spread on these surfaces and organized the cadherins into adhesive structures on the coverslip surface (Fig. S3), similar to published results (Gavard et al., 2004), whereas cell adhesion to control slides was negligible (not depicted). VEGFR3-GFP showed distinct colocalization with VEcad^{WT} compared with VEcad$^{N\text{-}TMD}$, providing further evidence for their interaction in cells.

Direct binding between TMDs

We next addressed whether the VEcad–VEGFR interaction was direct. For this purpose, we developed constructs containing the cadherin and VEGFR TMDs with short intracellular and extracellular tags for expression and purification from bacteria (sequences are provided in the Materials and methods). The recombinant VE- and N-TMD constructs were Flag-tagged, whereas the VEGFR2- and VEGFR3-TMDs were HA-tagged (Fig. 3 C, top). These peptides were purified in a nondenaturing CHAPS buffer, mixed, and incubated at 37°C, then immunoprecipitated with anti-HA beads. Blotting for Flag-tagged cadherin TMDs revealed that the VE-TMD bound both VEGFR2-TMD and VEGFR3-TMD but not the related PDGFRβ-TMD, whereas the N-TMD showed only background binding (Fig. 3 C, bottom). These results show that the VEcad and VEGFR complexes bind directly, and, moreover, that VEGFR2 and -3 show similar affinity.

The VEcad–VEGFR complex promotes shear-mediated VEGFR transactivation

Flow induces ligand-independent activation of VEGFR2, which is required for subsequent activation of PI3K and integrins (Jin et al., 2003; Tzima et al., 2005). We therefore tested whether flow also transactivates VEGFR3. To allow a direct comparison in these experiments, we used an antibody that recognizes phosphorylated Y1054/9 in the kinase domain activation loops, a site that is highly conserved between VEGFR2 and -3. Thus, anti-pY1054/9 does not discriminate between the two paralogues. HUVECs were subjected to short-term laminar shear and Y1054/9 phosphorylation was analyzed. Both VEGFR2 and VEGFR3 were initially activated similarly, but VEGFR3 exhibited a more sustained response (Fig. 4 A). The activation kinetics of each receptor were confirmed with additional phospho-VEGFR antibodies, anti-VEGFR2^{pY1175} and anti-VEGFR3^{pY1230}, which recognize sites commonly phosphorylated in response to ligand (Fig. 4 A). Thus, VEGFR3, like VEGFR2, shows activation by flow in the absence of ligand.

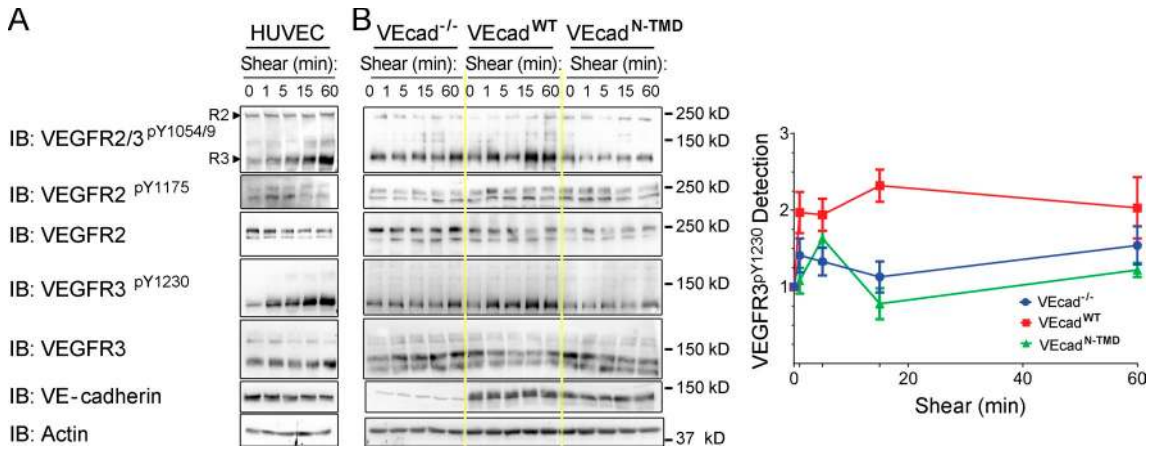

Figure 4. **VEcad TMD in shear-mediated VEGFR2 and VEGFR3 activation.** (A) VEGFR activation. HUVECs exposed to 12 dynes/cm^2 laminar shear for the indicated times were immunoblotted with the indicated antibodies. The upper band on the anti-VEGFR2/3$^{pY1054/9}$ blot is active VEGFR2; the lower band is active VEGFR3 (arrowheads). IB, immunoblotting. (B) Dependence on TMD. VEcad$^{-/-}$, VEcad^{WT}, and VEcad$^{\Delta TMD}$ cells were subjected to shear stress, then lysed and immunoblotted as in A. The anti-VEGFR^{pY1230} blots were quantified by densitometry of the ~120-kD band with actin serving as a loading control. Values are means ± SEM (error bars), $n \geq 3$. Yellow lines mark boundaries between cell types.

Next, we tested the dependence of VEGFR activation on the VEcad TMD by examining VEcad$^{-/-}$, VEcad^{WT}, and VEcad$^{N\text{-}TMD}$ cells. Shear-mediated activation of VEGFR2 and -3 required the VEcad TMD (Fig. 4 B). Additionally, we assayed effects of the VEcad TMD on VEGFR2 activation in response to its ligand, VEGF-A165. WT VEcad enhanced VEGFR2^{pY1175} activation by VEGF-A above the levels seen in VEcad$^{-/-}$ cells (Fig. S4 A); VEcad$^{N\text{-}TMD}$ enhanced VEGFR2 activation nearly as effectively as WT VEcad at early times of stimulation, though VEGFR2 activation decreased faster than with WT. These data indicate that the TMD interaction is not required for the initial enhancement of VEGF responses by VEcad but that it influences maintenance of the signal at later times. Similar results were obtained in HUVEC shRNA/rescue experiments (Fig. S4 B).

VEGFRs display functional overlap and dosage sensitivity

These results raise questions about the relative contribution of VEGFR2 and -3 in flow signaling. Published functional analyses (Jin et al., 2003; Tzima et al., 2005) used chemical inhibitors of tyrosine kinase activity that do not discriminate between these paralogues (Eskens and Verweij, 2006), thus, it is unclear to what extent VEGFR2 and -3 have unique effectors, and function additively or redundantly. VEGFR2 is required for shear-mediated activation of PI3K and integrins, and for cell alignment. We therefore performed shear experiments with human ECs treated with siRNAs against each VEGFR, or both (Fig. 5 A). Depletion of the individual VEGFRs partially decreased phosphorylation of PI3K and had a slight effect on Akt activation, as determined by immunoblotting pS473 (Warfel et al., 2011), whereas depletion of both strongly inhibited it (Fig. 5, B and C). Therefore, VEGFR2 and -3 both contribute to shear-mediated PI3K-Akt signaling.

When alignment after 16 h of flow was assayed, depletion of either VEGFR2 or VEGFR3 substantially inhibited alignment, whereas depletion of both receptors slightly increased the degree of inhibition (Fig. 6). Next, depletion was rescued using adenoviruses containing mCherry (control, −), VEGFR2-GFP, or VEGFR3-GFP to express each paralogue at levels close to endogenous (Fig. S5 A). VEGFR2-GFP rescued not only its own knockdown but also knockdown of VEGFR3; similarly, VEGFR3-GFP rescued both its own and VEGFR2 knockdown (Fig. 6). These results show that while both VEGFR2 and VEGFR3 contribute to flow signaling, they are functionally redundant. Different downstream pathways show different dose requirements, but the effects appear to be essentially additive. In support of this conclusion, we estimated the ratio of endogenous VEGFR2/VEGFR3 in HUVEC to be ~2:1 by calibrating anti-VEGFR antibodies with VEGFR2-GFP and VEGFR3-GFP constructs, with anti-GFP as a reference antibody (Fig. S5 B).

VEcad-VEGFRs in inflammatory flow signaling

The junctional complex is required for flow stimulation of inflammatory pathways that lead to leukocyte recruitment (Liu et al., 2008), a key step in initiation of atherosclerosis. Activation of fibronectin-binding integrins and subsequent activation of NF-κB are critical components of this response (Orr et al., 2005; Liu et al., 2008). We therefore tested the role of the VEGFRs in these events. Integrin activation was assayed by incubating cells with a recombinant, GST-tagged fibronectin fragment consisting of the ninth to eleventh FN repeats (GST-FN9-11). The flow-induced increase in GST-FN9-11 binding was completely blocked by depletion of either VEGFR (Fig. 7 A). Maximal activation of the integrins with Mn^{2+} completely reversed the effects of VEGFR depletion, ruling out loss of integrin expression or surface localization. Thus, both VEGFR2 and VEGFR3 are required for shear-induced integrin activation. We also assayed events downstream of NF-κB. Up-regulation of the leukocyte adhesion receptor VCAM-1 in response to oscillatory shear stress (OSS) was strongly inhibited by depletion of either VEGFR2 or -3 (Fig. 7 B). Consistent with this result, stimulation of monocyte adhesion by OSS was also almost completely inhibited by siRNA against VEGFR2 or VEGFR3 individually (Fig. 7 C).

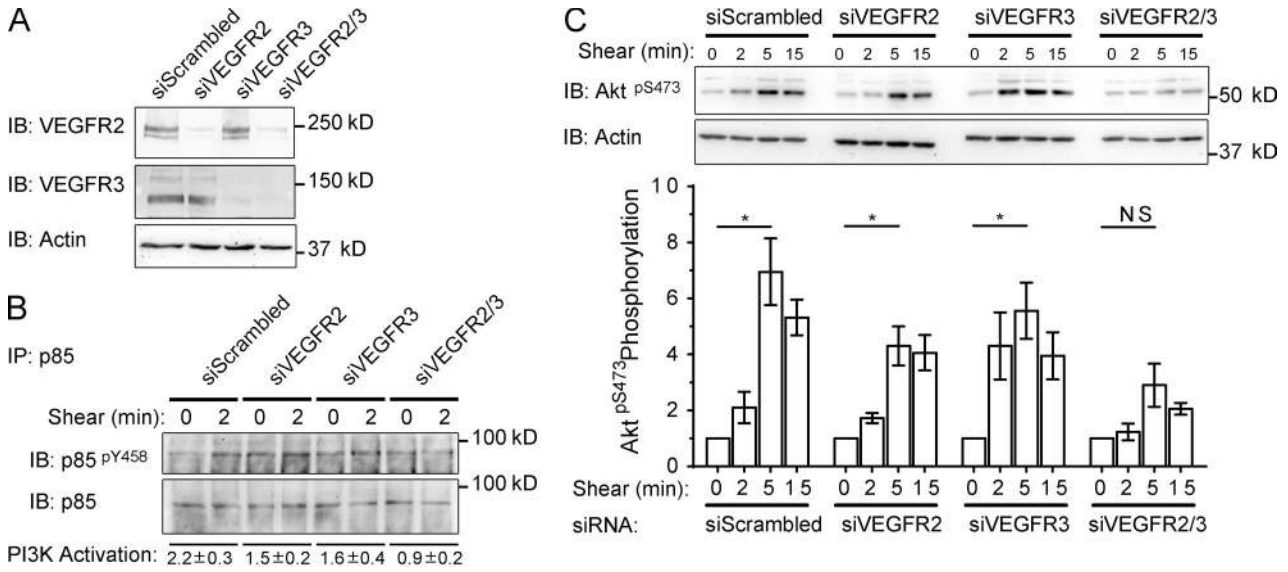

Figure 5. **VEGFRs in PI 3-kinase and integrin activation.** (A) VEGFR knockdown. HUVECs transfected with the indicated siRNAs for 72 h were analyzed for VEGFR expression by immunoblotting. Three independent experiments gave similar results. (B) PI3K signaling. HUVECs transfected as in A were subjected to shear stress and p85 was immunoprecipitated. Samples were then analyzed by immunoblotting and densitometry as in Fig 2 C. Values are means ± SEM, $n = 4$. (C) Akt signaling. siRNA-treated HUVECs were subjected to laminar shear stress for the indicated times and lysates were analyzed by immunoblotting with the indicated antibodies to determine Akt activity. Results were quantified by densitometry, with actin serving as a loading control. Values are means ± SEM (error bars), $n = 3$. *, $P < 0.05$ relative to unstimulated cells by two-way ANOVA. IB, immunoblotting.

We then tested the requirement for the VEcad–VEGFR interaction in shear-induced inflammatory signaling by applying OSS to $VEcad^{WT}$ and $VEcad^{N\text{-}TMD}$ cells. Oscillatory shear activated NF-κB and up-regulated VCAM-1 in $VEcad^{WT}$ cells but not in $VEcad^{N\text{-}TMD}$ cells (Fig. 7 D). Therefore, the VEGFRs must associate with VEcad in order for endothelial cells to respond to OSS.

VEGFR3 contributes to shear signaling in vivo

Last, we sought to address the role of VEGFR3 in flow signaling in vivo. VEGFR3 is expressed in lymphatic endothelial cells (Karkkainen et al., 2000) and angiogenic endothelium (Kubo et al., 2000; Gu et al., 2001; Witmer et al., 2001; Tammela et al., 2008) but its expression is relatively weak in quiescent adult arteries. We therefore hypothesized that VEGFR3 expression might be correlated with activated endothelium/sites of vascular remodeling. Thus, we first examined VEGFR3 expression in arterial endothelium by qPCR of mRNA isolated from endothelial cell in adult mouse aortas. VEGFR3 expression was easily detected in this assay (Fig. 8 A). Next, we examined mice in which YFP was knocked into the VEGFR3 locus to generate a VEGFR3 reporter (Calvo et al., 2011). Longitudinal sections of aortas from adult mice showed robust YFP expression in the inner curvature of the aortic arch, with weaker expression throughout the rest of the aorta (Fig. 8 B and data not depicted). No fluorescence was observed in control mice lacking YFP expression. Interestingly, the inner curvature is a site where disturbed flow induces chronic inflammation in WT mice, characterized by the accumulation of fibronectin and VCAM-1 within the intima, which primes the endothelium for development of atherosclerosis in hypercholesterolemia (Davies et al., 2013). To test the role for VEGFR3 in disturbed flow–induced inflammatory activation of the endothelium, we used an inducible VEGFR3 deletion model. Adult male *Cdh5:Cre*, *Vegfr3*$^{lox/lox}$, and WT control mice were treated with tamoxifen to induce VEGFR3 excision (Fig. 8 B). After 3 wk, VEGFR3 deletion reduced staining for fibronectin (Fig. 8 D) and VCAM-1 (Fig. 8 E) in the inner curvature of the aortic arch compared with their WT counterparts. These data show that VEGFR3 contributes to shear-induced inflammatory signaling in vivo.

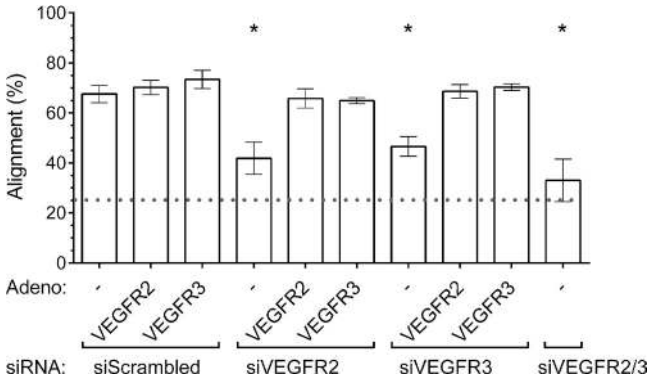

Figure 6. **VEGFRs in shear-induced alignment.** HUVECs were transfected with siRNAs as in Fig 4 A before being infected with mCherry (−) or VEGFR-expressing adenoviruses as indicated. Cells were subject to 12 dynes/cm^2 laminar shear stress for 16 h. Then, fixed cell alignment was quantified as in Fig 1 B. Values are means ± SEM (error bars), $n \geq 3$. *, $P < 0.05$ relative to siScramble by one-way ANOVA. The broken line indicates random alignment, as in Fig. 1.

Discussion

VEcad is structurally and functionally very similar to other classical cadherins but is unique in its contribution to flow sensing by endothelial cells (Tzima et al., 2005). In this study, we used

Ncad and VEcad chimeras to identify the sequences required for shear stress mechanotransduction. This approach led to the surprising result that the TMD is the critical VEcad-specific sequence. This conclusion is supported by both loss-of-function and gain-of-function constructs, which indicates that in the context of a functional classical cadherin, the TMD is both necessary and sufficient for flow signaling. The VEcad TMD primary sequence contains unique, conserved features distinct from both Ncad and more similar type II cadherins (unpublished data). These results add to the growing literature showing that these previously ignored domains serve as more than just membrane anchors (Andersen and Koeppe, 2007; Moore et al., 2008; Cosson et al., 2013). Recent studies have shown that TMDs determine subcellular distribution, protein clustering, and membrane microdomain localization (Sharpe et al., 2010; Bocharov et al., 2012; Diaz-Rohrer et al., 2014). Transmembrane protein–protein interactions additionally control the activation status of receptor tyrosine kinases, integrins, and channels (Therien et al., 2001; DiMaio and Petti, 2013; Endres et al., 2013; Manni et al., 2014). The role of the VEcad TMD in mechanotransduction thus extends this list in a new direction.

Next, we found that the VEcad TMD mediates binding to VEGFRs 2 and 3, which, based on assays with purified TMD constructs, is direct. VEcad was previously shown to co-immunoprecipitate with VEGFR2, and to modulate VEGFR2 downstream signaling in response to VEGF to decrease Erk and increase PI3K (Carmeliet et al., 1999). VEcad and VEGFR2 were also found to interact in flow signaling, where they co-immunoprecipitate and where VEcad was required for ligand-independent activation of VEGFR2 by flow (Tzima et al., 2005). These new data therefore show that the TMDs for VEcad and VEGFR2 mediate their interaction.

The results also identify VEGFR3 as a novel component of the junctional complex. Like VEGFR2, VEGFR3 was activated by the onset of shear stress and signaled through PI3K and integrins in a VEcad-TMD–dependent manner. Knockdown and rescue experiments showed that these VEGFRs are functionally redundant, as each can rescue loss of the other. This feature is unexpected because otherwise VEGFR2 and -3 induce distinct endothelial fates (arterial vs. lymphatic) during development (Olsson et al., 2006). This difference may reflect ligand-dependent versus ligand-independent signaling, or may reflect our incomplete understanding of the downstream pathways that mediate these fate decisions. In any case, the data further suggest that what matters in flow signaling is total receptor expression levels. HUVECs in culture express comparable levels of VEGFR2 and -3 (Fig. S5 B). Knockdown experiments showed that depletion of either receptor individually strongly reduced flow-induced integrin activation, cell alignment, and inflammatory activation; had a partial effect on PI3K; and had a weak effect on Akt. However, depletion of both receptors strongly inhibited all of these effector functions. Thus, these differences can be explained simply if different downstream events have different dose requirements.

Finally, we tested a functional role for VEGFR3 in mice in flow-dependent mechanotransduction. VEGFR3 is normally expressed in blood vessels during development and adult

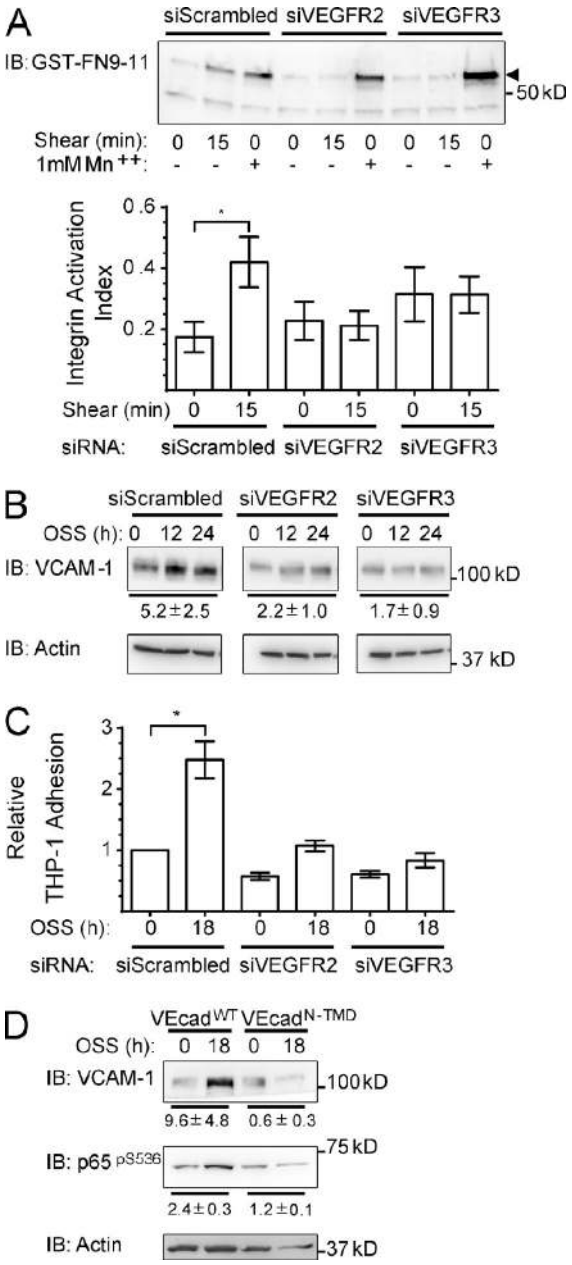

Figure 7. **The VEcad–VEGFR complex in inflammatory signaling.** (A) Integrin activation. HUVECs transfected with the indicated siRNA were left untreated or exposed to 15 min of laminar shear stress. After shear stress, slides were incubated with GST-FN9-11. Mn^{2+} was used as a positive control to maximally active the integrins. Bound GST-FN9-11 was detected by immunoblotting with anti-GST and quantified by densitometry. Graphed values are means ± SEM (error bars; $n = 4$) after normalization to Mn^{2+}. *, $P < 0.05$ using a Student's t test. The arrowhead indicates full-length, active GST-FN9-11 protein. (B) VCAM-1 induction. siRNA-transfected cells were exposed to OSS for 12–24 h. Lysates were collected and immunoblotted with anti–VCAM-1 and anti-actin. Bands were quantified by densitometry and values are expressed as means ± SEM, $n = 3$, relative to the unstimulated condition. (C) Monocyte binding. HUVECs were exposed to OSS as in B for 18 h, then incubated with THP-1 monocytes in HBSS+BSA for 30 min. Slides were washed, fixed, and stained. Bound monocytes were then quantified by fluorescence microscopy. Values are means ± SEM (error bars), $n = 3$, normalized to unstimulated siScrambled. *, $P < 0.05$ using a Student's t test. (D) Dependence on TMD. $VEcad^{WT}$ and $VEcad^{N\text{-}TMD}$ cells were exposed to OSS for 18 h, then analyzed for VCAM-1 expression and NF-κB p65 activation, with actin as a loading control. Bands were quantified by densitometry. Values are means ± SEM, $n = 4$, relative to unstimulated controls. IB, immunoblotting.

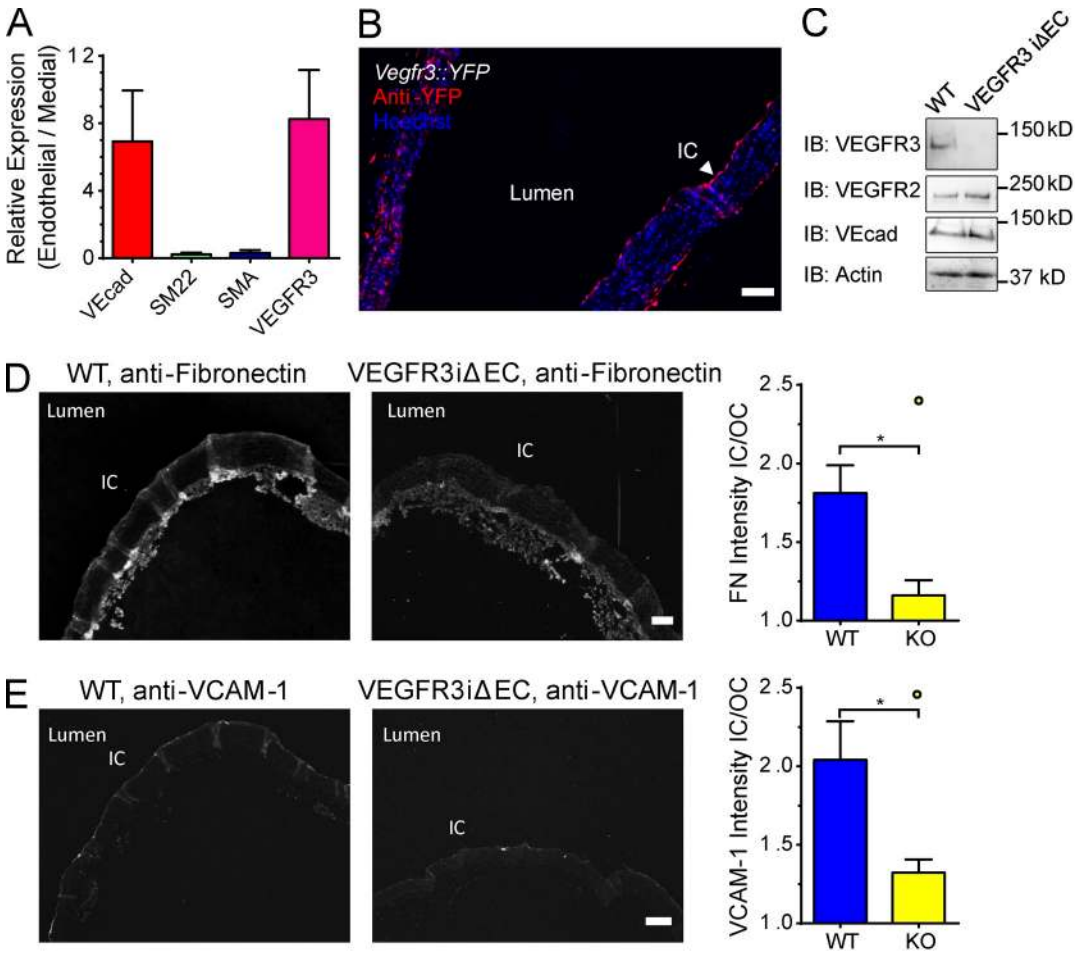

Figure 8. **The role of VEGFR3 in the mouse aorta.** (A) VEGFR3 expression in arterial endothelium. Total RNA isolated from the endothelial layer was analyzed by qPCR for the indicated genes. VEcad and VEGFR3 expression are represented as mean fold enrichment of the endothelial preparation over the remaining media ± SEM (error bars) from four aortas. The relative abundance of the medial layer markers SMA and SM22 indicate the purity of endothelial preparations. (B) VEGFR3 reporter. Aortas from adult VEGFR3-driven YFP gene reporter mice were sectioned longitudinally and stained for the YFP reporter and for nuclei using Hoechst staining. IC, inner curvature. Images are representative of five mice from several litters. (C) VEGFR2 iΔEC. Endothelial-specific, inducible VEGFR3 knockout (iΔEC) and WT control mice were treated with tamoxifen, and aortas were removed after 1 wk. Tissue lysates were collected and immunoblotted with the indicated antibodies. IB, immunoblotting. (D and E) Inflammatory markers. VEGFR3 iΔEC and WT control mice were treated with tamoxifen and examined at 3 wk. Aortas were sectioned longitudinally and stained for fibronectin (D) or VCAM-1 (E). Images are representative of 6 mice from two independent experiments. Bars, 100 µm. The ratio of mean fluorescence intensity between the inner and outer curvature was then quantified. Values are means ± SEM (error bars). *, $P < 0.05$. Open circles denote outliers excluded from analysis by Grubbs' test ($\alpha = 0.05$).

angiogenesis but is otherwise low in stable arteries (Gu et al., 2001; Witmer et al., 2001; Tammela et al., 2008). However, we found that its mRNA was readily detectable in the normal mouse aorta, and a reporter construct was up-regulated at the inner curvature of the aortic arch that is exposed to disturbed shear stress. The subsequent chronic inflammatory activation of the endothelium in these regions "primes" the vessel for development of atherosclerosis under conditions of high cholesterol (Jongstra-Bilen et al., 2006). Deletion of VEGFR3 in adult mice reduced inflammatory signaling at this site. No loss of lymphatic vessels was noted after VEGFR3 deletion (unpublished data). Moreover, the circulating levels for VEGF-C, the ligand for VEGFR3, are negligible (Joukov et al., 1996), which is consistent with ligand-independent activation. We conclude that VEGFR3 significantly contributes to flow signaling in vivo. Interestingly, others have previously noted that deletion of VEGFR3 during development causes severe vascular abnormalities that are not phenocopied by deletion of the two known VEGFR3 ligands VEGF-C and VEGF-D (Haiko et al., 2008). Thus, shear stress–mediated VEGFR3 signaling may also contribute to developmental vascular remodeling.

VEcad was previously placed in a flow signaling pathway downstream of SFKs and upstream of PI3K (Tzima et al., 2005). Here we show that VEcad contributes to this pathway through its role as an adaptor for VEGFRs. Interestingly, cadherins are known to indirectly associate with SFKs through catenins (Piedra et al., 2003). Because previous reports have shown that VEGFR2 and VEGFR3 transactivation is SFK-dependent and ligand-independent (Jin et al., 2003; Galvagni et al., 2010), we hypothesize that VEcad could be involved in bringing together SFKs with VEGFRs in order to facilitate the phosphorylation of the latter by the former. In contrast, VEGFR activation by $VEGFA_{165}$ was only modestly dependent on the VEcad-TMD, mainly at later times. The timing of this effect suggests that it

may be caused by effects of VEcad on VEGFR trafficking, which is known to control downstream signaling (Lampugnani et al., 2006). However, complete loss of VEcad had a stronger effect on VEGF responses. Other sequences in VEcad therefore appear to contribute to VEGFR signaling in ways that remain to be elucidated. The membrane phosphatase VE-PTP is a good candidate, as it directly binds VEcad and regulates VEGFR signaling (Nawroth et al., 2002). In summary, these results provide new molecular understanding of how VEcad functions in mechanotransduction. They demonstrate that the VEcad TMD mediates an adapter function through binding to VEGFR TMDs to facilitate ligand-independent transactivation. They also identify VEGFR3 as a component of the junctional mechanosensory complex, and demonstrate an additive relationship between VEGFR2 and -3. Major unanswered questions for future work include elucidating the relationship to PECAM-1 in mechanotransduction and understanding in detail how, and which, SFK members promote VEcad-mediated VEGFR activation.

Materials and methods

Cloning

Human VEcad, human Ncad, and mouse VEcad cDNAs were used to make C-terminally Flag-tagged chimeras in a modified pBOB lentiviral expression vector. The following amino acid sites were used to make chimeras: $VE^{1–623}$-$N^{747–906}$ ($VE^{ECD+TMD}$); $VE^{622–784}$-$N^{1–747}$ (VE^{ICD}); $N^{1–504}$-$VE^{380–623}$-$N^{747–906}$ ($VE^{CA4-5+TMD}$); $N^{1–504}$-$VE^{383–480}$-$N^{607–906}$ (VE^{CA4}); $N^{1–605}$-$VE^{482–622}$-$N^{747–906}$ ($VE^{CA5+TMD}$); $N^{1–717}$-$VE^{595–622}$-$N^{747–906}$ (VE^{TMD}); and Mm_$VE^{1–594}$-$N^{717–747}$-$VE^{622–784}$ (VE^{N-TMD}). Bacterial expression constructs were prepared by annealing oligonucleotides encoding peptide fragments and subcloning into a modified pET expression vector. Human and mouse VEGFR2-GFP and VEGFR3-GFP were cloned into adenoviral and lentiviral, CMV-driven expression vectors using LR clonase (Gateway system; Invitrogen) between pENTR1A and pAd/CMV/V5-DEST or pLenti6/V5-DEST.

Cell culture

VEcad–null embryoid body–derived endothelial cells ($VEcad^{-/-}$) were maintained in DMEM, 20% FBS, 1× endothelial cell growth supplement (ECGS), 100 mg/liter heparin, and 1× penicillin/streptomycin. HUVECs were obtained from the Yale tissue culture core, cultured in M199, 20% FBS, 1× ECGS, 100 mg/liter heparin, and 1× penicillin/streptomycin, and used at passage 1–6. ECGS was prepared by homogenizing and clarifying bovine hypothalamus (Pel-Freez Biologicals) as described previously (Maciag et al., 1979).

Antibodies and reagents

The following antibodies were used for immunoblotting throughout this study: rabbit anti-Flag (#2368; Cell Signaling Technology) and goat anti-VEcad (C-19; Santa Cruz Biotechnology, Inc.). Total and phospho-VEGFRs were detected with rabbit anti-VEGFR2 (#2479; Cell Signaling Technology), goat anti-HsVEGFR3 (AF349; R&D Systems), goat anti-MmVEGFR3 (AF743; R&D Systems), rabbit anti-$VEGFR2^{pY1175}$ (#2478; Cell Signaling Technology), rabbit anti-$VEGFR^{pY1054/9}$ (44-1047G; Invitrogen), and rabbit anti-$VEGFR3^{pY1230/1}$ (CY1115; Cell Applications). Other phospho-antibodies used for immunoblotting include rabbit anti-SFK^{pY416} (#6943; Cell Signaling Technology), rabbit anti-$p85^{pY458}$ (#4228; Cell Signaling Technology), rabbit anti-Akt^{pS473} (700392; Invitrogen), and rabbit ant-$p65^{pS536}$ (#3033; Cell Signaling Technology). Anti–VCAM-1 was obtained from Abcam (ab134047). Loading control antibodies include rabbit anti–β-Actin (N-21; Santa Cruz Biotechnology, Inc.), rabbit anti-p85 (06-497; EMD Millipore), goat anti-HA (#ab9134; Abcam), rabbit anti–β-Catenin (#9562; Cell Signaling Technology), rabbit anti-GFP (A11122; Invitrogen), and mouse anti-Tubulin (DM1A; Sigma-Aldrich). Human VEGF-A165 was obtained from R&D Systems (293-VE-010).

Viral infection

Lentiviral expression plasmids were cotransfected with pVSVG and psPAX2 packaging plasmids into HEK-293T cells with Lipofectamine 2000 (Life Technologies). Viral supernatants were collected and used to infect $VEcad^{-/-}$ cells in the presence of 10 µg/ml polybrene. 48 h after infection, cells were assayed for protein expression and subjected to cell panning on anti-VEcad–coated dishes or FACS sorting to enrich the infected population as necessary.

siRNAs

HUVECs were transferred into endothelial growth media (Lonza) for 24 h, then cells at ∼75% confluency were transfected with 10 nM final ON-Target Smartpool siRNAs (L-003138 and L-003148 from GE Healthcare; AM4636 from Ambion) complexed with RNAiMAX (Invitrogen). VEGFR2 siRNA, 5′-GGGCAUGUACUGACGAUUA-3′, 5′-CUACAUUGUUCUUCCGAUA-3′, 5′-GGAAAUCUCUUGCAAGCUA-3′, and 5′-GCGAUGGCCUCUUCUGUAA-3′; VEGFR3 siRNA, 5′-CGCCCGAGUUCCAGUGGUA-3′, 5′-GAACUUGACCGACCUCCUG-3′, 5′-GCGAAUACCUGUCCUACGA-3′, and 5′-GCAAGAACGAUCUGUU-3′. Cells were maintained in transfection media for 24 h, then returned to standard M199 base media. Experiments were performed 72–90 h after transfection. For adenoviral rescue, cells were infected with virus and 5 µg/ml polybrene 36 h after siRNA transfection.

Immunoprecipitation

Confluent HUVECs in complete medium were rinsed with PBS containing 1 mM Ca^{2+} and 0.5 mM Mg^{2+}, then lysed with cold 25 mM Tris, pH 7.5, 600 mM NaCl, 0.3% CHAPS (3023; Sigma-Aldrich), 0.15% Triton X-100, 1.5× PhosSTOP (Roche), and 1.5× Protease inhibitor (Roche) at 1 ml/10^6 cells. Lysates were drawn through a 23G syringe 15 times and incubated on ice for 30 min before clarification at 20,000 *g* for 10 min. Clarified lysates were immunoprecipitated with either anti-Flag resin (Sigma-Aldrich) or Protein A/G beads (Santa Cruz Biotechnology, Inc.) bound to anti-cadherin (VEcad, BV9 [Santa Cruz Biotechnology, Inc.]; Ncad, 610920 [BD]) or VEGFR (VEGFR2, 55B11 [Cell Signaling Technologies]; VEGFR3, AF349 [R&D Systems]) antibodies, as indicated, for 2.5 h at 4°C. Beads were washed three times with 1 ml of lysis buffer. Flag immunoprecipitates were eluted at 4°C for 60 min in lysis buffer with 0.2 mg/ml 3×-flag peptide (Sigma-Aldrich). Eluted proteins were then collected in protein sample buffer (PSB), then analyzed by SDS-PAGE and immunoblotting with chemiluminescent HRP detection.

p85 immunoprecipitation. Cells were lysed in 25 mM Tris, pH 7.5, 200 mM NaCl, 1% Triton X-100, 0.5% deoxycholate, 1.5× PhosSTOP, and 1.5× Protease inhibitor for 30 min on ice before clarification at 20,000 *g*. Immunoprecipitation was performed with anti–p85-bound Protein A/G beads at 4°C for 6 h. Beads were then washed four times with 1 ml of lysis buffer, eluted in PSB, and analyzed by SDS-PAGE and immunoblotting with anti-$p85^{pY458}$.

In vitro binding

Synthetic cDNAs encoding either Flag-tagged (cadherin) or HA-tagged (receptor tyrosine kinase) TMDs were constructed in a modified pET28 vector for bacterial expression. Flag-VE-TMD, MAAAAGSDYKDDDDKGCPGGNASVSIQAVVAILLCILTITVITLLIFLRRRSGGLNDIFEAQKIEWHESSEFEFEHHHHHH*; Flag-N-TMD, MAAAAGSDYKDDDDKGCPGGNASGAIIAILLCIIILLILVLMFVVWMKRRSGGLNDIFEAQKIEWHESSEFEFEHHHHHH*; HA-VEGFR2-TMD, MAAAAGSYPYDVPDYAGCPGGNASLEIIILVGTAVIAMFFWLLLVIILRTVKRRSGGDSLEFIASKLAGSEFEFEHHHHHH*; HA-VEGFR3-TMD, MAAAAGSYPYDVPDYAGCPGGNASMEIVILVGTGVIAVFFWVLLLLIFCNMRRSGGDSLEFIASKLAGSEFEFEHHHHHH*; HA-PDGFRβ-TMD, MAAAAGSYPYDVPDYAGCPGGNASLTVAAAVLVLLVIVIISLIVLVVIWKRSGGDSLEFIASKLAGSEFEFEHHHHHH*. Asterisks indicate stop codons/C terminus. Constructs were transformed into BL21 cells. Cultures were expanded in super broth at 37°C before shifting to 30°C and inducing protein expression with 50 µM IPTG for 5 h. Bacteria were pelleted and frozen at −80°C. Pellets were resuspended in 50 mM Tris, pH 7.5, 150 mM NaCl, 0.1% CHAPS, 0.2% Triton X-100, 1× protease inhibitor, 0.25 mM DTT, 5 mM imidazole, and 1.5 mg/ml lysozyme, incubated on ice for 15 min, then sonicated three times with 30 500-ms pulses at 50% output. Lysates were clarified by centrifugation at 20,000 *g* for 20 min. Supernatants were incubated with Ni^{2+}-NTA resin for 1 h at 4°C, then beads were washed four times and eluted for 2 h, at 4°C, with 300 mM imidazole. For each binding reaction, ∼1 µg of HA-tagged proteins were captured with Protein A/G resin, prebound with HA.11 monoclonal antibody (Covance). Resin was then washed and equilibrated in binding buffer containing 25 mM Tris, pH 7.5, 300 mM NaCl, 0.3% CHAPS, 0.15% Triton X-100, 0.25 mM DTT, and 1× protease inhibitor at 37°C. Then, eluted Flag-tagged cadherin TMD were diluted to 20 µg/ml in binding buffer, warmed to 37°C for 30 min,

and clarified at 20,000 *g*. The HA-bound resin and Flag-tagged peptides were rotated at 37°C for 2.5 h, washed three times with 37°C binding buffer, and eluted in PSB. Blots were then performed with rabbit anti-Flag (CST) and goat anti-HA antibodies.

Shear stress alignment

Cells were seeded on plastic-coated cell culture–treated slides with 10 µg/ml bovine fibronectin for ∼24 h, clamped into a 25 × 55 mm parallel plate flow chamber (Frangos et al., 1988), and sheared at 12 dynes/cm^2 in complete media for 16 h. Cells were fixed in 3.7% formaldehyde and stained with either anti-Flag (2368; Cell Signaling Technology) or anti–VEcad (C19; Santa Cruz Biotechnology, Inc.), Alexa Fluor 647–phalloidin (Molecular Probes), and Hoechst (Molecular Probes). Slides were mounted in fluoromount-G (SouthernBiotech). Fluorescence microscopy was performed at room temperature with a microscope (80i; Nikon) equipped with 10× (NA 0.45) and 20× (NA 0.75) objective lenses and a CCD camera (Retiga 200R; QImaging). Images were collected throughout the length of the slide with NIS Elements software. Cells were then scored for alignment within ±23° of the axis of shear using ImageJ.

Oscillatory flow and monocyte adhesion

Reconstituted VEcad$^{-/-}$ cells were starved in 2% FBS, 0.1× ECGS for 72 h. HUVEC were starved in 5% FBS, 0.25× ECGS for 8 h. Cells in parallel plate chambers were subjected to oscillatory shear at 1 ± 3 dynes/cm^2 at 1 Hz for 18 h by applying flow from a motorized syringe pump (NE-1050; New Era) and a peristaltic pump (Microflex; Cole-Palmer), as described previously (Orr et al., 2005). To assay monocyte adhesion, THP-1 suspension cultures were resuspended in HBSS, 1 mM Ca^{2+}, 0.5 mM Mg^{2+}, and 0.5% BSA, and added to the slides with HUVECs. After 30 min at 37°C, slides were washed four times in HBSS with cations and fixed with 3.7% formaldehyde. Cells were stained with anti–VEcad (C19; Santa Cruz Biotechnology, Inc.), phalloidin, and Hoechst before fluorescence microscopy. A 10× objective lens was used to capture 8–12 random images from the center of the slide and bound monocytes were counted per image. Data were normalized relative to siScrambled, and static and multiple independent experiments were used to obtain mean-fold changes with SEM.

Short-term shear

For shear <60 min, cells were starved for 18 h in media containing 2% FBS, 0.1× ECGS, then exposed to 12 dynes/cm^2 laminar shear for the indicated times. Cells were rinsed in PBS, snap-frozen at −80°C, and thawed into cold RIPA buffer, and lysates were clarified as before. For VEGFR activation, triplicate slides were combined for each time point.

Integrin activation assays

GST-FN9-11 in pGEX was induced in BL21 cells and purified according to standard procedures into TBS-Tween buffer. Protein was desalted to remove Tween and diluted to 20 µg/ml in TBS containing 0.5% BSA and either 1 mM Ca^{2+}, 1 mM Mg^{2+}, or 1 mM Mn^{2+}. Starved cells were sheared at 12 dynes/cm^2 for 15 min, rinsed, and incubated with GST-FN at 37°C for 30 min. Slides were washed in RT buffer three times for 5 min each with gentle agitation. Cells were then lysed in PSB, then analyzed by SDS-PAGE and immunoblotting for GST (#2625; Cell Signaling Technology).

RNA isolation and qPCR

Intimal RNA isolation was performed according to Nam et al. (2009). In brief, C57BL/6 mice were euthanized and perfused with saline through the left ventricle. Aortic sections between the arch and thoracic region were isolated and cleared of periadventitial tissue before eluting the endothelium with 250 µl of QIAzol (QIAGEN) perfused through an insulin syringe. RNA from the endothelium and remaining media were then isolated and amplified with miRNeasy mini using whole transcriptome amplification kits (QIAGEN) according to the manufacturer's instructions. cDNA was then used for real-time quantitative PCR in a real-time PCR detection system (CFX96; Bio-Rad Laboratories) using iQ-SYBRGreen supermix (Bio-Rad Laboratories). VEGFR3 was amplified with QIAGEN primer set QT01744848. Other primers include SMA Fwd, ATCGTCCACCGCAAATGC; and Rev, AAGGAACTGGAGGCGCTG; SM22 Fwd, GCGCCTGGGCTTCCA, and Rev, CAGGCTGTTCACCAATTTGCT; VECAD Fwd, CACTGCTTTGGGAGCCTTC, and Rev, GGGGCAGCGATTCATTTTTCT; and B2M Fwd, CCGAGCCCAAGACCGTCTA, and Rev, AACTGGATTTGTAATTAAGCAGGTTCA. The normalized ratios of messages within the endothelial elutes from individual aortas were then quantified and graphed in Prism (GraphPad Software).

Vegfr3 reporter and deletion experiments

Vegfr3::YFP mice were created by homologous recombination of a BAC clone, modified by inserting YFP within exon 1 of a VEGFR3 allele, as previously described (Calvo et al., 2011). These mice have been backcrossed extensively with C57BL/6. To access *Vegfr3::YFP* expression, mice were sacrificed at 2–4 mo and fixed by perfusion with 3.7% formaldehyde. The aorta was removed, cleared of periadventitial tissue, and further fixed overnight at 4°C. Aortas were then embedded in paraffin and sectioned longitudinally by the Yale Pathology Tissue Microarray facility. *Vegfr3$^{flox/flox}$* mice were created previously by targeting the exon/intron1 of the *Vegfr3* locus with a neomycin cassette bounded by loxP and frt sites and crossing mice with β-actin–driven FLPe recombinase (Haiko et al., 2008). These mice have been backcrossed extensively with C57BL/6. To generate endothelial-specific inducible *Vegfr3* knockout mice, *Vegfr3$^{flox/flox}$* mice were crossed with *Cdh5^{CreERT2}* mice (Pitulescu et al., 2010; Wang et al., 2010). At 6–8 wk of age, *Vegfr3$^{flox/flox}$* mice, with or without the Cre recombinase, were then injected intra-peritoneally with 2 mg tamoxifen (Sigma-Aldrich) prepared in peanut oil (Sigma-Aldrich) with 10% ethanol on five consecutive days. For ex vivo protein analysis, the aorta was dissected 1 wk after tamoxifen injection and cleared of connective tissue and adventitia. Proteins were extracted with a denaturating extraction buffer containing 9.5 M urea, 1% NP-40, 5% β-mercaptoethanol, 1% pharmalytes (pI: 3–10), and proteases inhibitors and clarified by 20,000 *g* centrifugation. For immunohistological analysis, mice were sacrificed 3 wk after Cre induction and aortas were collected. All experiments were approved by the Institutional Animal Care and Use Committee of Yale University.

Immunohistochemistry

Paraffin was removed in xylene baths and sections were progressively rehydrated before antigen retrieval for 30 min at 95°C in citrate buffer (10 mM sodium citrate, 0.05% Tween, pH 6). Sections were then blocked for 30 min in StartingBlock (Thermo Fisher Scientific) and probed either with anti-GFP antibody (#A11122 [Invitrogen], overnight at 4°C, 1:400), anti-fibronectin antibody (#3648 [Sigma-Aldrich], 1 h at RT, 1:500), or anti-VCAM1 antibody (#ab134047 [Abcam], overnight at 4°C, 1:400). Slides were washed three times in PBS-Tween, once in PBS, and stained with donkey anti–rabbit Alexa Fluor 647 secondary antibody for 1 h at RT, at 1:500. Slides were washed as before then mounted with Fluoromount G (Southern Biotech). Samples were imaged with a microscope (80i; Nikon) as described for the shear experiments. To quantify, 10× images were used to determine the mean fluorescence intensity of the endothelial layer of the inner and outer curvatures defined as signal at a depth of ∼15 µm from the lumen. Background signal was measured within the lumen and subtracted. The ratio of inner curvature/outer curvature per mouse was calculated and graphed using Prism.

Online supplemental material

Fig. S1 illustrates similar expression, junctional localization, and catenin binding of cadherin chimeras in reconstituted VEcad$^{-/-}$ cells. Fig. S2 shows the negligible influence of shear stress in the stability of the mechanosensory complex and the similar binding characteristics of VEGFR2 as compared with binding of VEGFR3 shown in Fig. 3 B. Fig. S3 illustrates colocalization of VEcad with VEGFR3 in cells spread on Fc-VE^{ECD}. Fig. S4 shows the responsiveness of VEcad-reconstituted cells to VEGF-A stimulation. VEcad$^{N\text{-}TMD}$ reconstituted cells show a partial, time-dependent rescue of VEGFR2 activation. Fig. S5 shows the extent of VEGFR2/3 expression in the rescue experiments performed as part of Fig. 6 and the blotting strategy used to determine relative expression levels of VEGFR paralogues. Online supplemental material is available at http://www.jcb.org/cgi/content/full/jcb.201408103/DC1.

The authors would like to thank Pascal and Laurence Fragner for generation of VEGFR-GFP expression vectors, Dr. Kasey Baker for assistance performing preliminary mouse experiments, Dr. Yongli Zhang for technical advice, and Dr. Bruno Larrivee for assisting in adenovirus experiments. The Yale W.M. Keck facilities provided oligo synthesis, DNA sequencing, and proteomic services. The Yale Pathology Tissue Microarray facility provided support in tissue preparation.

This work was funded by National Institutes of Health grant 5R01HL075092 to M.A. Schwartz and by fellowships from National Institutes of Health (5T32HL007950) and the American Heart Association (13POST16720007) to B.G. Coon.

The authors declare no competing financial interests.

Author contributions: B.G. Coon and M.A. Schwartz designed the experiments, analyzed the data, and wrote the paper. N. Baeyens, J. Han, and

M. Budatha conducted animal experiments and immunohistochemistry. T.D. Ross and N. Baeyens contributed to data analysis. J.S. Fang, S. Yun, and J.-L. Thomas helped prepare essential reagents.

Submitted: 26 August 2014
Accepted: 12 February 2015

References

Andersen, O.S., and R.E. Koeppe II. 2007. Bilayer thickness and membrane protein function: an energetic perspective. *Annu. Rev. Biophys. Biomol. Struct.* 36:107–130. http://dx.doi.org/10.1146/annurev.biophys.36.040306.132643

Bocharov, E.V., K.S. Mineev, M.V. Goncharuk, and A.S. Arseniev. 2012. Structural and thermodynamic insight into the process of "weak" dimerization of the ErbB4 transmembrane domain by solution NMR. *Biochim. Biophys. Acta*. 1818:2158–2170. http://dx.doi.org/10.1016/j.bbamem.2012.05.001

Calvo, C.F., R.H. Fontaine, J. Soueid, T. Tammela, T. Makinen, C. Alfaro-Cervello, F. Bonnaud, A. Miguez, L. Benhaim, Y. Xu, et al. 2011. Vascular endothelial growth factor receptor 3 directly regulates murine neurogenesis. *Genes Dev.* 25:831–844. http://dx.doi.org/10.1101/gad.615311

Carmeliet, P., M.G. Lampugnani, L. Moons, F. Breviario, V. Compernolle, F. Bono, G. Balconi, R. Spagnuolo, B. Oosthuyse, M. Dewerchin, et al. 1999. Targeted deficiency or cytosolic truncation of the VE-cadherin gene in mice impairs VEGF-mediated endothelial survival and angiogenesis. *Cell*. 98:147–157. http://dx.doi.org/10.1016/S0092-8674(00)81010-7

Chiu, J.J., and S. Chien. 2011. Effects of disturbed flow on vascular endothelium: pathophysiological basis and clinical perspectives. *Physiol. Rev.* 91:327–387. http://dx.doi.org/10.1152/physrev.00047.2009

Chiu, Y.J., E. McBeath, and K. Fujiwara. 2008. Mechanotransduction in an extracted cell model: Fyn drives stretch- and flow-elicited PECAM-1 phosphorylation. *J. Cell Biol.* 182:753–763. http://dx.doi.org/10.1083/jcb.200801062

Chiu, J.J., S. Usami, and S. Chien. 2009. Vascular endothelial responses to altered shear stress: pathologic implications for atherosclerosis. *Ann. Med.* 41:19–28. http://dx.doi.org/10.1080/07853890802186921

Cicha, I., M. Goppelt-Struebe, A. Yilmaz, W.G. Daniel, and C.D. Garlichs. 2008. Endothelial dysfunction and monocyte recruitment in cells exposed to non-uniform shear stress. *Clin. Hemorheol. Microcirc.* 39:113–119.

Conway, D.E., M.T. Breckenridge, E. Hinde, E. Gratton, C.S. Chen, and M.A. Schwartz. 2013. Fluid shear stress on endothelial cells modulates mechanical tension across VE-cadherin and PECAM-1. *Curr. Biol.* 23:1024–1030. http://dx.doi.org/10.1016/j.cub.2013.04.049

Cosson, P., J. Perrin, and J.S. Bonifacino. 2013. Anchors aweigh: protein localization and transport mediated by transmembrane domains. *Trends Cell Biol.* 23:511–517. http://dx.doi.org/10.1016/j.tcb.2013.05.005

Dai, G., M.R. Kaazempur-Mofrad, S. Natarajan, Y. Zhang, S. Vaughn, B.R. Blackman, R.D. Kamm, G. García-Cardeña, and M.A. Gimbrone Jr. 2004. Distinct endothelial phenotypes evoked by arterial waveforms derived from atherosclerosis-susceptible and -resistant regions of human vasculature. *Proc. Natl. Acad. Sci. USA*. 101:14871–14876. http://dx.doi.org/10.1073/pnas.0406073101

Davies, P.F. 1995. Flow-mediated endothelial mechanotransduction. *Physiol. Rev.* 75:519–560.

Davies, P.F., M. Civelek, Y. Fang, and I. Fleming. 2013. The atherosusceptible endothelium: endothelial phenotypes in complex haemodynamic shear stress regions in vivo. *Cardiovasc. Res.* 99:315–327. http://dx.doi.org/10.1093/cvr/cvt101

Diaz-Rohrer, B.B., K.R. Levental, K. Simons, and I. Levental. 2014. Membrane raft association is a determinant of plasma membrane localization. *Proc. Natl. Acad. Sci. USA*. 111:8500–8505. http://dx.doi.org/10.1073/pnas.1404582111

Di Stefano, I., D.R. Koopmans, and B.L. Langille. 1998. Modulation of arterial growth of the rabbit carotid artery associated with experimental elevation of blood flow. *J. Vasc. Res.* 35:1–7. http://dx.doi.org/10.1159/000025559

DiMaio, D., and L.M. Petti. 2013. The E5 proteins. *Virology*. 445:99–114. http://dx.doi.org/10.1016/j.virol.2013.05.006

Endres, N.F., R. Das, A.W. Smith, A. Arkhipov, E. Kovacs, Y. Huang, J.G. Pelton, Y. Shan, D.E. Shaw, D.E. Wemmer, et al. 2013. Conformational coupling across the plasma membrane in activation of the EGF receptor. *Cell*. 152:543–556. http://dx.doi.org/10.1016/j.cell.2012.12.032

Eskens, F.A., and J. Verweij. 2006. The clinical toxicity profile of vascular endothelial growth factor (VEGF) and vascular endothelial growth factor receptor (VEGFR) targeting angiogenesis inhibitors; a review. *Eur. J. Cancer*. 42:3127–3139. http://dx.doi.org/10.1016/j.ejca.2006.09.015

Feaver, R.E., B.D. Gelfand, C. Wang, M.A. Schwartz, and B.R. Blackman. 2010. Atheroprone hemodynamics regulate fibronectin deposition to create positive feedback that sustains endothelial inflammation. *Circ. Res.* 106:1703–1711. http://dx.doi.org/10.1161/CIRCRESAHA.109.216283

Fleming, I., B. Fisslthaler, M. Dixit, and R. Busse. 2005. Role of PECAM-1 in the shear-stress-induced activation of Akt and the endothelial nitric oxide synthase (eNOS) in endothelial cells. *J. Cell Sci.* 118:4103–4111. http://dx.doi.org/10.1242/jcs.02541

Frangos, J.A., L.V. McIntire, and S.G. Eskin. 1988. Shear stress induced stimulation of mammalian cell metabolism. *Biotechnol. Bioeng.* 32:1053–1060. http://dx.doi.org/10.1002/bit.260320812

Galvagni, F., S. Pennacchini, A. Salameh, M. Rocchigiani, F. Neri, M. Orlandini, F. Petraglia, S. Gotta, G.L. Sardone, G. Matteucci, et al. 2010. Endothelial cell adhesion to the extracellular matrix induces c-Src-dependent VEGFR-3 phosphorylation without the activation of the receptor intrinsic kinase activity. *Circ. Res.* 106:1839–1848. http://dx.doi.org/10.1161/CIRCRESAHA.109.206326

Gavard, J., M. Lambert, I. Grosheva, V. Marthiens, T. Irinopoulou, J.F. Riou, A. Bershadsky, and R.M. Mège. 2004. Lamellipodium extension and cadherin adhesion: two cell responses to cadherin activation relying on distinct signalling pathways. *J. Cell Sci.* 117:257–270. http://dx.doi.org/10.1242/jcs.00857

Giampietro, C., A. Taddei, M. Corada, G.M. Sarra-Ferraris, M. Alcalay, U. Cavallaro, F. Orsenigo, M.G. Lampugnani, and E. Dejana. 2012. Overlapping and divergent signaling pathways of N-cadherin and VE-cadherin in endothelial cells. *Blood*. 119:2159–2170. http://dx.doi.org/10.1182/blood-2011-09-381012

Gimbrone, M.A. Jr., and G. García-Cardeña. 2013. Vascular endothelium, hemodynamics, and the pathobiology of atherosclerosis. *Cardiovasc. Pathol.* 22:9–15. http://dx.doi.org/10.1016/j.carpath.2012.06.006

Goel, R., B.R. Schrank, S. Arora, B. Boylan, B. Fleming, H. Miura, P.J. Newman, R.C. Molthen, and D.K. Newman. 2008. Site-specific effects of PECAM-1 on atherosclerosis in LDL receptor-deficient mice. *Arterioscler. Thromb. Vasc. Biol.* 28:1996–2002. http://dx.doi.org/10.1161/ATVBAHA.108.172270

Gu, W., T. Brännström, W. Jiang, A. Bergh, and P. Wester. 2001. Vascular endothelial growth factor-A and -C protein up-regulation and early angiogenesis in a rat photothrombotic ring stroke model with spontaneous reperfusion. *Acta Neuropathol.* 102:216–226.

Hahn, C., and M.A. Schwartz. 2009. Mechanotransduction in vascular physiology and atherogenesis. *Nat. Rev. Mol. Cell Biol.* 10:53–62. http://dx.doi.org/10.1038/nrm2596

Hahn, C., A.W. Orr, J.M. Sanders, K.A. Jhaveri, and M.A. Schwartz. 2009. The subendothelial extracellular matrix modulates JNK activation by flow. *Circ. Res.* 104:995–1003. http://dx.doi.org/10.1161/CIRCRESAHA.108.186486

Hahn, C., C. Wang, A.W. Orr, B.G. Coon, and M.A. Schwartz. 2011. JNK2 promotes endothelial cell alignment under flow. *PLoS ONE*. 6:e24338. http://dx.doi.org/10.1371/journal.pone.0024338

Haiko, P., T. Makinen, S. Keskitalo, J. Taipale, M.J. Karkkainen, M.E. Baldwin, S.A. Stacker, M.G. Achen, and K. Alitalo. 2008. Deletion of vascular endothelial growth factor C (VEGF-C) and VEGF-D is not equivalent to VEGF receptor 3 deletion in mouse embryos. *Mol. Cell. Biol.* 28:4843–4850. http://dx.doi.org/10.1128/MCB.02214-07

Harry, B.L., J.M. Sanders, R.E. Feaver, M. Lansey, T.L. Deem, A. Zarbock, A.C. Bruce, A.W. Pryor, B.D. Gelfand, B.R. Blackman, et al. 2008. Endothelial cell PECAM-1 promotes atherosclerotic lesions in areas of disturbed flow in ApoE-deficient mice. *Arterioscler. Thromb. Vasc. Biol.* 28:2003–2008. http://dx.doi.org/10.1161/ATVBAHA.108.164707

Hove, J.R., R.W. Köster, A.S. Forouhar, G. Acevedo-Bolton, S.E. Fraser, and M. Gharib. 2003. Intracardiac fluid forces are an essential epigenetic factor for embryonic cardiogenesis. *Nature*. 421:172–177. http://dx.doi.org/10.1038/nature01282

Hwang, J., A. Saha, Y.C. Boo, G.P. Sorescu, J.S. McNally, S.M. Holland, S. Dikalov, D.P. Giddens, K.K. Griendling, D.G. Harrison, and H. Jo. 2003. Oscillatory shear stress stimulates endothelial production of O2- from p47phox-dependent NAD(P)H oxidases, leading to monocyte adhesion. *J. Biol. Chem.* 278:47291–47298. http://dx.doi.org/10.1074/jbc.M305150200

Jin, Z.G., H. Ueba, T. Tanimoto, A.O. Lungu, M.D. Frame, and B.C. Berk. 2003. Ligand-independent activation of vascular endothelial growth factor receptor 2 by fluid shear stress regulates activation of endothelial nitric oxide synthase. *Circ. Res.* 93:354–363. http://dx.doi.org/10.1161/01.RES.0000089257.94002.96

Jongstra-Bilen, J., M. Haidari, S.N. Zhu, M. Chen, D. Guha, and M.I. Cybulsky. 2006. Low-grade chronic inflammation in regions of the normal mouse arterial intima predisposed to atherosclerosis. *J. Exp. Med.* 203:2073–2083. http://dx.doi.org/10.1084/jem.20060245

Joukov, V., K. Pajusola, A. Kaipainen, D. Chilov, I. Lahtinen, E. Kukk, O. Saksela, N. Kalkkinen, and K. Alitalo. 1996. A novel vascular endothelial growth factor, VEGF-C, is a ligand for the Flt4 (VEGFR-3) and KDR (VEGFR-2) receptor tyrosine kinases. *EMBO J.* 15:290–298.

Karkkainen, M.J., R.E. Ferrell, E.C. Lawrence, M.A. Kimak, K.L. Levinson, M.A. McTigue, K. Alitalo, and D.N. Finegold. 2000. Missense mutations interfere with VEGFR-3 signalling in primary lymphoedema. *Nat. Genet.* 25:153–159. http://dx.doi.org/10.1038/75997

Kubo, H., T. Fujiwara, L. Jussila, H. Hashi, M. Ogawa, K. Shimizu, M. Awane, Y. Sakai, A. Takabayashi, K. Alitalo, et al. 2000. Involvement of vascular endothelial growth factor receptor-3 in maintenance of integrity of endothelial cell lining during tumor angiogenesis. *Blood*. 96:546–553.

Lampugnani, M.G., F. Orsenigo, M.C. Gagliani, C. Tacchetti, and E. Dejana. 2006. Vascular endothelial cadherin controls VEGFR-2 internalization and signaling from intracellular compartments. *J. Cell Biol.* 174:593–604. http://dx.doi.org/10.1083/jcb.200602080

Langille, B.L., and F. O'Donnell. 1986. Reductions in arterial diameter produced by chronic decreases in blood flow are endothelium-dependent. *Science*. 231:405–407. http://dx.doi.org/10.1126/science.3941904

Liu, Y., D.T. Sweet, M. Irani-Tehrani, N. Maeda, and E. Tzima. 2008. Shc coordinates signals from intercellular junctions and integrins to regulate flow-induced inflammation. *J. Cell Biol.* 182:185–196. http://dx.doi.org/10.1083/jcb.200709176

Lucitti, J.L., E.A. Jones, C. Huang, J. Chen, S.E. Fraser, and M.E. Dickinson. 2007. Vascular remodeling of the mouse yolk sac requires hemodynamic force. *Development*. 134:3317–3326. http://dx.doi.org/10.1242/dev.02883

Maciag, T., J. Cerundolo, S. Ilsley, P.R. Kelley, and R. Forand. 1979. An endothelial cell growth factor from bovine hypothalamus: identification and partial characterization. *Proc. Natl. Acad. Sci. USA*. 76:5674–5678. http://dx.doi.org/10.1073/pnas.76.11.5674

Manni, S., K.S. Mineev, D. Usmanova, E.N. Lyukmanova, M.A. Shulepko, M.P. Kirpichnikov, J. Winter, M. Matkovic, X. Deupi, A.S. Arseniev, and K. Ballmer-Hofer. 2014. Structural and functional characterization of alternative transmembrane domain conformations in VEGF receptor 2 activation. *Structure*. 22:1077–1089. http://dx.doi.org/10.1016/j.str.2014.05.010

Mattsson, E.J., T.R. Kohler, S.M. Vergel, and A.W. Clowes. 1997. Increased blood flow induces regression of intimal hyperplasia. *Arterioscler. Thromb. Vasc. Biol.* 17:2245–2249. http://dx.doi.org/10.1161/01.ATV.17.10.2245

Moore, D.T., B.W. Berger, and W.F. DeGrado. 2008. Protein-protein interactions in the membrane: sequence, structural, and biological motifs. *Structure*. 16:991–1001. http://dx.doi.org/10.1016/j.str.2008.05.007

Nam, D., C.W. Ni, A. Rezvan, J. Suo, K. Budzyn, A. Llanos, D. Harrison, D. Giddens, and H. Jo. 2009. Partial carotid ligation is a model of acutely induced disturbed flow, leading to rapid endothelial dysfunction and atherosclerosis. *Am. J. Physiol. Heart Circ. Physiol.* 297:H1535–H1543. http://dx.doi.org/10.1152/ajpheart.00510.2009

Navarro, P., L. Ruco, and E. Dejana. 1998. Differential localization of VE- and N-cadherins in human endothelial cells: VE-cadherin competes with N-cadherin for junctional localization. *J. Cell Biol.* 140:1475–1484. http://dx.doi.org/10.1083/jcb.140.6.1475

Nawroth, R., G. Poell, A. Ranft, S. Kloep, U. Samulowitz, G. Fachinger, M. Golding, D.T. Shima, U. Deutsch, and D. Vestweber. 2002. VE-PTP and VE-cadherin ectodomains interact to facilitate regulation of phosphorylation and cell contacts. *EMBO J.* 21:4885–4895. http://dx.doi.org/10.1093/emboj/cdf497

Nayak, L., Z. Lin, and M.K. Jain. 2011. "Go with the flow": how Krüppel-like factor 2 regulates the vasoprotective effects of shear stress. *Antioxid. Redox Signal.* 15:1449–1461. http://dx.doi.org/10.1089/ars.2010.3647

Nigro, P., J. Abe, and B.C. Berk. 2011. Flow shear stress and atherosclerosis: a matter of site specificity. *Antioxid. Redox Signal.* 15:1405–1414. http://dx.doi.org/10.1089/ars.2010.3679

Olsson, A.K., A. Dimberg, J. Kreuger, and L. Claesson-Welsh. 2006. VEGF receptor signalling - in control of vascular function. *Nat. Rev. Mol. Cell Biol.* 7:359–371. http://dx.doi.org/10.1038/nrm1911

Orr, A.W., J.M. Sanders, M. Bevard, E. Coleman, I.J. Sarembock, and M.A. Schwartz. 2005. The subendothelial extracellular matrix modulates NF-κB activation by flow: a potential role in atherosclerosis. *J. Cell Biol.* 169:191–202. http://dx.doi.org/10.1083/jcb.200410073

Orr, A.W., M.H. Ginsberg, S.J. Shattil, H. Deckmyn, and M.A. Schwartz. 2006. Matrix-specific suppression of integrin activation in shear stress signaling. *Mol. Biol. Cell*. 17:4686–4697. http://dx.doi.org/10.1091/mbc.E06-04-0289

Orr, A.W., C. Hahn, B.R. Blackman, and M.A. Schwartz. 2008. p21-activated kinase signaling regulates oxidant-dependent NF-κB activation by flow. *Circ. Res.* 103:671–679. http://dx.doi.org/10.1161/CIRCRESAHA.108.182097

Osawa, M., M. Masuda, K. Kusano, and K. Fujiwara. 2002. Evidence for a role of platelet endothelial cell adhesion molecule-1 in endothelial cell mechanosignal transduction: is it a mechanoresponsive molecule? *J. Cell Biol.* 158:773–785. http://dx.doi.org/10.1083/jcb.200205049

Piedra, J., S. Miravet, J. Castaño, H.G. Pálmer, N. Heisterkamp, A. García de Herreros, and M. Duñach. 2003. p120 Catenin-associated Fer and Fyn tyrosine kinases regulate β-catenin Tyr-142 phosphorylation and β-catenin-α-catenin interaction. *Mol. Cell. Biol.* 23:2287–2297. http://dx.doi.org/10.1128/MCB.23.7.2287-2297.2003

Pitulescu, M.E., I. Schmidt, R. Benedito, and R.H. Adams. 2010. Inducible gene targeting in the neonatal vasculature and analysis of retinal angiogenesis in mice. *Nat. Protoc.* 5:1518–1534. http://dx.doi.org/10.1038/nprot.2010.113

Pohl, U., J. Holtz, R. Busse, and E. Bassenge. 1986. Crucial role of endothelium in the vasodilator response to increased flow in vivo. *Hypertension*. 8:37–44. http://dx.doi.org/10.1161/01.HYP.8.1.37

Privratsky, J.R., D.K. Newman, and P.J. Newman. 2010. PECAM-1: conflicts of interest in inflammation. *Life Sci.* 87:69–82. http://dx.doi.org/10.1016/j.lfs.2010.06.001

Sharpe, H.J., T.J. Stevens, and S. Munro. 2010. A comprehensive comparison of transmembrane domains reveals organelle-specific properties. *Cell*. 142:158–169. http://dx.doi.org/10.1016/j.cell.2010.05.037

Stevens, H.Y., B. Melchior, K.S. Bell, S. Yun, J.C. Yeh, and J.A. Frangos. 2008. PECAM-1 is a critical mediator of atherosclerosis. *Dis. Model. Mech.* 1:175–181. http://dx.doi.org/10.1242/dmm.000547

Tammela, T., G. Zarkada, E. Wallgard, A. Murtomäki, S. Suchting, M. Wirzenius, M. Waltari, M. Hellström, T. Schomber, R. Peltonen, et al. 2008. Blocking VEGFR-3 suppresses angiogenic sprouting and vascular network formation. *Nature*. 454:656–660. http://dx.doi.org/10.1038/nature07083

Tedgui, A., and Z. Mallat. 2001. Anti-inflammatory mechanisms in the vascular wall. *Circ. Res.* 88:877–887. http://dx.doi.org/10.1161/hh0901.090440

Therien, A.G., F.E. Grant, and C.M. Deber. 2001. Interhelical hydrogen bonds in the CFTR membrane domain. *Nat. Struct. Biol.* 8:597–601. http://dx.doi.org/10.1038/89631

Tzima, E., M. Irani-Tehrani, W.B. Kiosses, E. Dejana, D.A. Schultz, B. Engelhardt, G. Cao, H. DeLisser, and M.A. Schwartz. 2005. A mechanosensory complex that mediates the endothelial cell response to fluid shear stress. *Nature*. 437:426–431. http://dx.doi.org/10.1038/nature03952

Vestweber, D. 2008. VE-cadherin: the major endothelial adhesion molecule controlling cellular junctions and blood vessel formation. *Arterioscler. Thromb. Vasc. Biol.* 28:223–232. http://dx.doi.org/10.1161/ATVBAHA.107.158014

Wang, Y., M. Nakayama, M.E. Pitulescu, T.S. Schmidt, M.L. Bochenek, A. Sakakibara, S. Adams, A. Davy, U. Deutsch, U. Lüthi, et al. 2010. Ephrin-B2 controls VEGF-induced angiogenesis and lymphangiogenesis. *Nature*. 465:483–486. http://dx.doi.org/10.1038/nature09002

Wang, C., B.M. Baker, C.S. Chen, and M.A. Schwartz. 2013. Endothelial cell sensing of flow direction. *Arterioscler. Thromb. Vasc. Biol.* 33:2130–2136. http://dx.doi.org/10.1161/ATVBAHA.113.301826

Warfel, N.A., M. Niederst, and A.C. Newton. 2011. Disruption of the interface between the pleckstrin homology (PH) and kinase domains of Akt protein is sufficient for hydrophobic motif site phosphorylation in the absence of mTORC2. *J. Biol. Chem.* 286:39122–39129. http://dx.doi.org/10.1074/jbc.M111.278747

Witmer, A.N., B.C. van Blijswijk, J. Dai, P. Hofman, T.A. Partanen, G.F. Vrensen, and R.O. Schlingemann. 2001. VEGFR-3 in adult angiogenesis. *J. Pathol.* 195:490–497. http://dx.doi.org/10.1002/path.969